PREDICTIVE MODELING

OF RESERVOIR RESPONSE TO HYDRAULIC STIMULATIONS

AT THE EUROPEAN EGS SITE SOULTZ-SOUS-FORÊTS

T. Kohl and T. Mégel

GEOWATT AG
Dohlenweg 28
CH-8050 Zürich; Switzerland
e-mail: kohl@geowatt.ch

ABSTRACT

With the beginning of the new century, the European EGS project got into its decisive state by reaching the final reservoir depth of 5 km. The three boreholes, GPK2, GPK3 and GPK4 have been successfully targeted at their predefined reservoir positions. Improvement of the reservoir conditions by stimulation with a minimized seismic risk represents now a primary challenge to enable economic operation and future extension. In this context, the new HEX-S code has been developed to simulate the transient hydro-mechanical response of the rock matrix to massive hydraulic injections. The present paper describes the successful forecast of the pressure response and shearing locations for the GPK4 stimulation in September 2004. As basis for this predictive modelling the reservoir model was derived from data analysis of the stimulation of GPK3 in May 2003. Stimulation flow rates up to 45 l/s at GPK4 and of >60 l/s at GPK3 have been applied, triggering several ten thousand of microseismic events. The transient numerical simulations with the HEX-S code match the main characteristics of both, the microseismic and the hydraulic behaviour. Different model calculations demonstrate the capabilities of our new approach. It is noteworthy that the modelling became possible only due to the excellent data quality at the Soultz project. The results demonstrate that simulations based on solid physical ground can reveal the complex reservoir behaviour during hydraulic stimulation. The use of HEX-S also provides perspectives for future developments such as design calculations that enable optimizing cost-intensive hydraulic stimulations before hand.

Keywords: numerical calculation; hydraulic stimulation; shearing; microseismicity

1 INTRODUCTION

The European Enhanced Geothermal System (EGS) project site at Soultz-sous-Forêts (France) is located in a nearly NNE-SSW striking Graben structure between the Vosges and Black Forest mountains to the East and West, north of Strasbourg (see also Fig. 1). The targeted heat exchanger is a granitic rock matrix, covered by Triassic and Tertiary sedimentary formations. The Graben system has been formed in

a period of strong extension in Late Eocene and Oligocene times. The topmost part of the horst structure developed locally at the Soultz site and its Triassic cover (Buntsandstein) are traversed by several large fault systems parallel to the Graben shoulder which are well known by oil exploration wells and partly even visible on the surface morphology. The fault systems parallel to the Graben have been repeatedly drilled during earlier project phases, such as the 'Soultz Fault' crossing the first borehole GPK1 in the Buntsandstein unit between 1000 and 1400 m and a major fault drilled in 2000 m depth at GPK2. Soultz is located at a major heat flow anomaly in the Rhine Graben, however, within a lateral few km distance surface heat flow can vary over several tenth of mW m^{-2} [1]. Vertically, a strong variation has been measured with values dropping from 150 mW m^{-2} at surface to <25 mW m^{-2} in 2-3 km depth and increasing again at greater depth to ~70 mW m^{-2} [2]. The reason for these variations are most probably natural convection in a fractured rock matrix with permeabilities of k>10^{-15}m^2 [3].
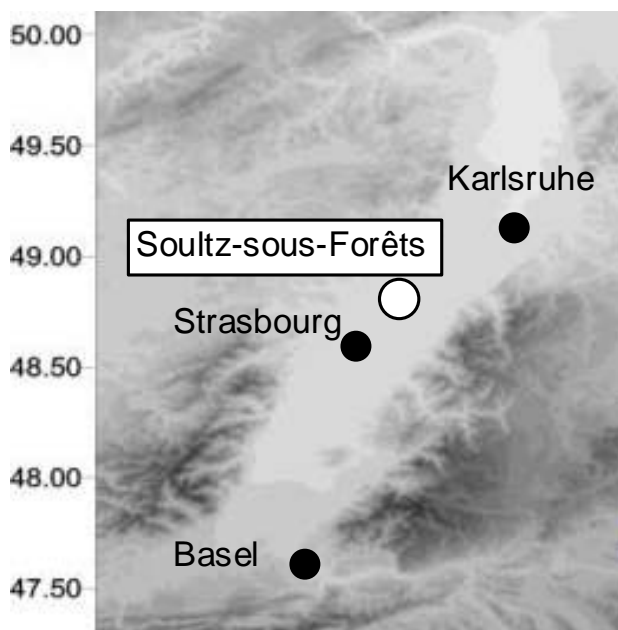

Fig. 1.   Location of Soultz-sous-Forêts, North of Strasbourg (France)

In the current exploration phase of the European EGS Project at Soultz-sous-Forêts the 5000 m deep reservoir in the crystalline basement is intended to form a module consisting of a central injector and two producer wells. The first well GPK2, drilled in 1999, is located most northward. The central injector well GPK3 was drilled in 2002 and targeted using the microseismic information from the former GPK2 stimulation. The third borehole, GPK4, drilled in 2004, was successfully directed into the planned location at >1 km south of the drilling platform. Details of the project are described by e.g. Baria et al. [4]. The planned triplet is aligned in roughly N-S direction, reflecting the normal/strike-slip stress regime at the Rhine-Graben location. The bottom hole temperature was 200.6 °C and separation between the wells at 5 km depth is around 700 m. The latest of the major stimulation tests took place in February 2005 at GPK4. Details of the current measurement program are described in Gérard [5].

Due to technical reasons, the fracture pattern at the deeper part of the GPK2 borehole can only be roughly estimated. However, different image tools have been applied to GPK3 and GPK4 and a

connection between fracture pattern and microseismicity can be established (see later). Therefore, the present paper is concentrating on the GPK3 and GPK4 hydraulic stimulations. These hydraulic stimulations have been conducted at GPK3 from 27 May to 6 June 2003 and at GPK4 from 13 to 16 September 2004. At GPK3, flow rate was varied in several steps up to > 60 l/s and more than 30'000 microseismic events have been recorded, whereas at GPK4 maximum flow rates of 45 l/s have been used. Kohl & Mégel [6] have illustrated the seismic response to flow rate changes with clear increasing activity at increasing flow rate and vice-versa. The connection between hydraulic and brittle elastic processes is obvious and has also been observed at various other locations and conditions. This evidence has led to the development of the HEX-S code. Especially, the code is focused on the simulation of the transient 3-D evolution of overpressure and shear events in the rock matrix in space and time.

The importance of shearing fractures on the hydraulic behaviour is well known. Barton et al. [7] describe in the classical paper the correlation between critically stressed faults and hydraulically conductive structures. Earlier Segall [8] observed the triggering of earthquakes from fluid extraction at oil fields and Maillot et al. [9] and Cuenot et al. [10] describe the occurrence of fluid induced micro-earthquakes with double couple focal mechanisms implying a dominant shear motion. However, only recently, the calculation of the coupled hydro-mechanical interaction occurring during hydraulic stimulation of a fractured rock matrix became a goal of investigations (i.e. [9], [11]). The herein presented approach is possibly the 1st one to calculate the poroelastic effects arising from a full 3-D hydraulic field on local fracture zones. The goal of the modelling with HEX-S is to provide a reliable physical explanation of the hydraulic and seismic events during hydraulic stimulation. Herewith, it is envisaged to model the hydraulic and seismic processes in a reservoir in a way that the complex non-linear processes are characterized on solid physical ground. Various theoretical test scenarios have been calculated already (e.g. [12-14]), however, this time the challenging task of a prognosis was intended.

2 MODELING CONCEPT

2.1 The hydro-mechanical code HEX-S

The hydro-mechanical code HEX-S has been developed to calculate the stimulation processes in a fractured reservoir during massive injection into a borehole. The code takes into account the aperture change of each fracture in the model due to the corresponding overpressure resulting from the injection. The propagation of the overpressure in the reservoir as well as the development of the anisotropic permeability in the fractured reservoir as a result of the fracture apertures is calculated as a time-dependent process. Poroelastic coupling is restricted to a fracture network. Our approach is in agreement with the results of stress inversion from microseismic events of Cornet & Jianmin [15] who observe that hydraulically active faults are related to local increase of pore pressure.

Hence the reaction of the reservoir permeability to an arbitrary injection rate history can be calculated. Towards the end of this paper, Fig. 16 illustrates the typical transient development and improvement of the reservoir by identifying an aperture change, Δa, of 0.1 mm in a fractured reservoir due to hydraulic injection.

Generation of the fracture network

The permeability distribution in a HEX-S model depends essentially on the location, orientation, aperture and extent of the incorporated fractures. HEX-S allows defining an arbitrary number of both, stochastic and deterministic, fracture sets. Experience from various EGS test sites demonstrates that microseismic events often follow planar structures (i.e. [16],[17], [10]). Since we assume that in most cases an induced microseismic event represents the shear failure of a part of a fracture surface area ("slip patch"), the locations of the calculated shearing events can be compared with the microseismic clouds. In contrary, possible mode I events (normal stress variations) remain unidentified.

In HEX-S every fracture or fracture zone is so far represented by a circular plane subdivided into a number of circular slip patches with small, predefined radii originating from seismic interpretation. The aperture of each specific slip patch contributes to the final permeability distribution in the model. Starting from an initial value (see below), the aperture change of a fracture depends on the orientation, the local effective stress field and its defined mechanical parameters.

Each fracture zone in HEX-S is defined either deterministically or stochastically, with following detailed properties:

1. Deterministic fracture zones consist of slip patches with explicitly defined positions, radii, orientations and classes of mechanical behaviour. The essential information is generally derived from borehole logs (e.g. FMS, UBI) but may also be the result of post-experimental interpretation of individual, microseismically active planar structures (Fig. 2).

2. Stochastically generated fracture zones have random locations and orientations. Input parameters for the stochastic generation are the statistical distribution of the orientation of fracture zones seen in borehole logs. Depending on the quality and degree of investigation only hydraulic active, major impedance anomalies or all traces can be used. Preferentially, our analysis uses the results of earlier sophisticated interpretation of hydraulic relevant features. For a specific starting value of a random sequence ("random seed number", RSN) a model with a specific distribution of fracture zone locations is generated. (Example of a specific distribution see Fig. 3). Each stochastically generated model, independent from the RSN has the same distribution of orientations of fracture zones. In the presented modeling stochastically generated fracture zones are used at locations with little information (i.e. at greater distance from the boreholes). The distribution and orientation is calculated from statistical evaluation of the observed fractures intersecting the boreholes. The herewith-defined model domain is filled-up until a predefined fracture (or slip patch) density is reached. The density should coincide with the accounted fracture traces. In the case of Soultz, sets of >20'000 slip patches are generated this way.

The initial aperture of each slip patch is proportional to its radius [18] and is calculated from the orientation to the local stress field. The final effective aperture distribution is scaled hydraulically in a way that each observation (i.e. generally the transmissivity of the open borehole section) is represented. The same procedure is used for each borehole. An average scaling factor is applied thereafter to control the effective aperture distribution in the reservoir. Clearly, this concept aims at the aperture determination along individual boreholes. For calibration of an initial hydraulic reservoir model, this represents only a first "guess" for the up-scaled permeability resulting from well a connected stochastic fracture network.

During a separate calibration procedure, model parameters are determined that allow better fitting results. The fracture density in the reservoir the coupling interaction scheme of the mechanical and hydraulic process will be explained below.
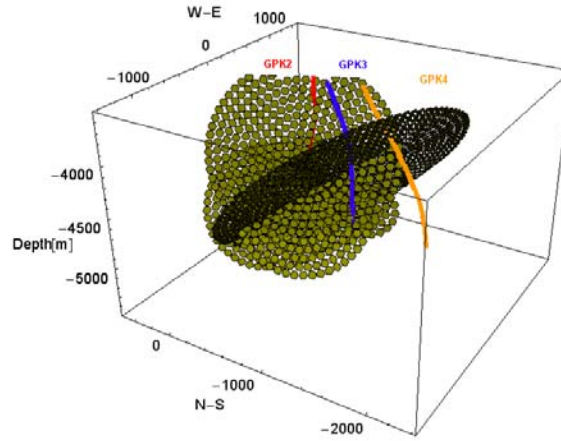

Fig. 2: *Example of a model with deterministic fracture zones (see Table 1 below) subdivided into slip patches for the 5 km deep reservoir domain at Soultz-sous-Forêts. Also indicated are the boreholes GPK2, GPK3 and GPK4*
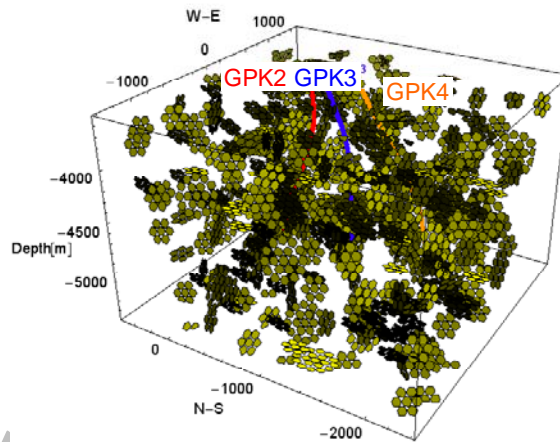

Fig. 3: *Example of one realization for stochastically generated fracture zones at the 5 km deep reservoir of Soultz-sous-Forêts. Also indicated are the boreholes GPK2, GPK and GPK4*

Implemented fracture aperture laws

The implemented aperture laws for the fractures or slip patches are basically of analytical kind ([18], [19], [20]). The aperture of a fracture depends on the following parameters: 1) the mechanical properties of the fracture, 2) the fluid pressure in the fracture space and 3) the normal and the shear stress on the fracture plane. The influence of overall elastic deformations in the entire rock matrix on the local permeability (i.e. aperture changes) and of heat and chemistry effects is not implemented so far.

The effective normal stress $\sigma_{n,eff}$ and the effective shear stress τ_{eff} on the plane of a fracture are derived from the three regional principal stress components and the fluid pressure, P, at the fracture location. Depending on the pore and fracture fluid pressure, the fracture aperture at a given location is assumed to be a function of three different opening processes:

a) Normal compliance only

Under the condition of low effective shear stress, τ_{eff}, only a compliant reaction of the fracture walls to fluid pressure will affect the aperture. This compliant aperture a_c is a function of an initial aperture under zero stress conditions, the effective normal stress $\sigma_{n,eff}$ and a 90%-closure stress $\sigma_{n,ref}$ (e.g. for $\sigma_{n,ref} = \sigma_{n,eff}$ the compliant aperture $a_c = a0/10$) defined as a specific fracture property:

$$a_c = \frac{a_0}{1 + 9\dfrac{\sigma_{n,eff}}{\sigma_{n,ref}}}$$

The initial aperture a_0 of each individual fracture is calibrated thus the totality of compliant fracture apertures a_c under the initial pore pressure and stress field fits the predefined permeability of the model.

The conditions for the compliant behaviour are

$$\sigma_{n,eff} > 0$$

$$\Delta\tau = \tau_{eff} - \sigma_{n,eff} \cdot \tan(\Phi) \quad < 0$$

(Mohr-Coulomb criterion)

As convention, stress is positive for compression. The friction angle Φ of the fracture walls is implemented as a function of $\sigma_{n,eff}$. The aperture increase is treated as reversible and vanishes as soon the pressure declines after the end of injection.

b) Compliance and shearing

If the effective shear stress τ_{eff} at the fracture walls exceeds the friction resistance, i.e. $\Delta\tau > 0$, and the effective normal stress $\sigma_{n,eff}$ still is positive, the fracture fails. The additional "shear" aperture change, a_s, due to the shear offset, U, is

$$a_s = U \cdot \tan(\Phi_{dil})$$

The shear dilation angle of the fracture wall, Φ_{dil}, is also implemented as function of $\sigma_{n,eff}$. The shear offset is defined from fracture shear stiffness, K_s, as:

$$U = \frac{\Delta\tau}{K_s}$$

This portion of the aperture increase is considered to be irreversible when injection test has stopped and the pressure field in the reservoir has reached its ambient value.

c) Jacking and shearing

In the case the effective normal stress, $\sigma_{n,eff}$, becomes negative, the fracture walls separate and the friction forces acting on them disappear. In addition to the shear aperture change (described above), a contribution from jacking conditions, a_j, arises. Clearly, a_j is considered to be fully reversible.

Although the shear induced, mode II, aperture change of a fracture is the only permanent effect after an injection test has ended, the contributions from jacking and compliance are also of major importance for the propagation of the pressure front during the stimulation process.

Hydraulic processes

The time-dependent pressure calculation in HEX-S is performed with a new finite element (FE) algorithm, which is a further development of the FRACTure code [21]. The main advantages of the FE algorithm are in efficient and flexible formulations:

- Local mesh refinement at specified locations in the reservoir domain such as boreholes

- Utilization of an implicit time-step procedure for transient calculation

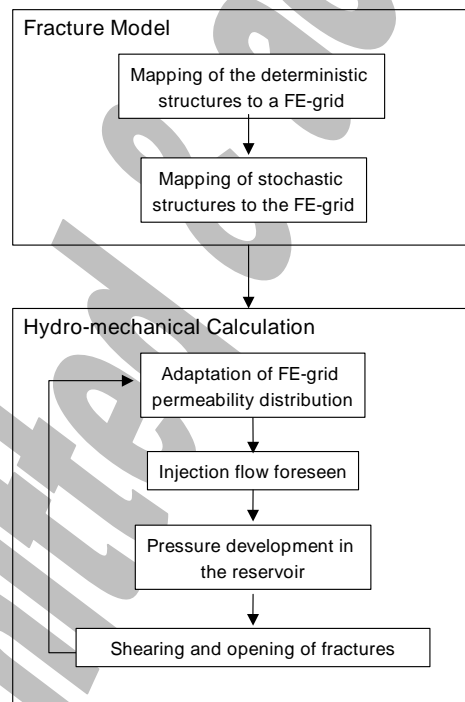- Easy extension to further physical processes or constitutive laws

Fig. 4: Principle flow chart of HEX-S

The hydraulic conductivity for each element is derived from the apertures of the intersecting slip patches by a specific mapping procedure. The intersection of the discrete fractures with the continuous FE grid is calculated using a "Rock-to-Fracture volumetric index", RFVI. The mapping results in individual FE

volumes of strongly anisotropic properties. Thereby, the hydraulic properties of the FE grid are modified after each time-step. HEX-S calculates the pressure in the model and determines the new apertures of the slip patches. When the hydraulic conductivities of the elements have been updated from the corresponding slip patch apertures, a next time-step is carried out (Fig. 4).

2.2 HEX-S Model of the 5km deep Soultz Reservoir

The FE- model used for the simulation of the hydro-mechanical processes in the 5 km deep Soultz reservoir consists of ~450'000 nodes, covering a surface area of 12x10 km^2 and a total depth range of 3000-6000 m. As general Soultz convention, the origin of the model (coordinates 0/0/0) is set to the head of the 3.5 km deep GPK1 borehole. The model is strongly refined towards its center, along the stimulated open-hole sections of GPK2, GPK3 and GPK4 between 4500-5000m depth. Fig. 5 illustrates this refinement in vertical and horizontal direction. Towards the boreholes, hexahedrons with partly less than 25x25x25m^3 have been applied. The hydraulic behavior along the open-hole sections of the boreholes is simulated using vertical 1D elements. In the modeling procedure, vertical boreholes had been assumed, each located near the top of the corresponding open hole section. The deviations to the real trajectories of GPK2 and GPK3 are minor, at the bottom part of GPK4 a lateral difference of ~100 m occurs however. Accordingly, the observed locations of the fractures at this part of GPK4 have been corrected for the deterministic fracture data. The hydraulic boundary conditions account for the large vertical fault zones in the Rhine Graben area. Hence, Dirichlet boundary conditions ($\Delta P=0$) best describe such drainage systems along the lateral borders. The injected flow is simulated as Neuman boundary condition at the top of the open-hole section (i.e. at the topmost part of the 1-D borehole element). The variation of flow rate is controlled in the model by load-time functions that allow specifying the transient change of boundary conditions at arbitrary time intervals.

In a compilation of R. Maurer [22], a total of 28 deterministic fractures intersecting the three boreholes were implemented into the HEX-S model (Table 1). The location of the hydraulically active fractures at GPK2 had to be determined by the BRGM (French Geological Survey) based on the analysis of flow logs. As UBI (Ultrasonic Borehole Imager) logs were not carried out in the open hole section of the GPK2 well, the orientation of the flowing fractures have been best-estimated by BRGM based on past experience of the deep-seated structures of the Soultz granite and on hydraulic data. In the GPK3 and GPK4 wells, UBI imaging along the entire granite section was performed. Relevant fracture parameters (depth, orientation, apparent aperture) have been also interpreted by BRGM. Along the open-hole sections, only the large and open fractures have been taken into account in the model. The position and orientation of the integrated deterministic fractures intersecting the boreholes are listed in Table 1. Most fractures are near-critically stressed. The data was established from apparently relevant fracture thickness with clear response on the transit time at UBI images on a preliminary evaluation from BRGM and from R. Maurer. The definitive characterization of the fracture date may be submitted to slight variations.

In addition to these deterministic fractures intersections, deterministic fault zones at larger distance - derived from the location of microseismic events - and stochastic fracture distributions in the intermediate rock matrix - calculated from the fracture distribution statistics - are included in the model. In total a gross number of >60'000 single slip patches are generated and accounted for.
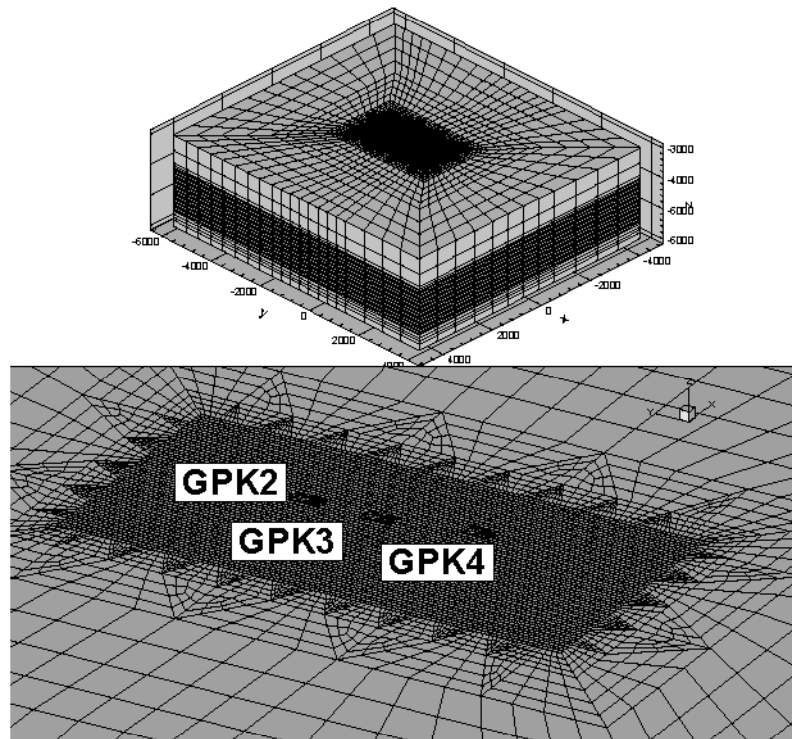
Fig. 5:   FE model for the reservoir domain in Soultz-sous-Forêts with the 5 km boreholes GPK2/3/4, used for the hydraulic calculations in HEX-S. Consisting of ~400'000 elements. North direction is aligned along the y-axis. The lower part illustrates a close view of the refinement at the model surface in 3 km depth.

Table 1: Integrated fracture data for GPK2, GPK3 and GPK4. The coordinates represent the fracture intersection with each borehole in the local Soultz coordinate system (origin at wellhead GPK1)

Borehole	x	y	z	azimuth of dip dip angle
GPK2	33.5	-438.7	-4394.8	250/70
GPK2	11.8	-419.5	-4458.5	70/70
GPK2	-6.4	-408.4	-4525.1	70/70
GPK2	-53.7	-376.6	-4716.8	250/65
GPK2	-79	-355.9	-4816.5	250/65
GPK2	-108.5	-337.8	-4936.6	250/70
GPK3	111.5	-956.8	-4517.4	122/66
GPK3	111.5	-956.8	-4517.7	124/61
GPK3	111.5	-957.1	-4542.3	330/54
GPK3	111.5	-957.1	-4542.6	320/54
GPK3	111.4	-957.3	-4569.1	307/60
GPK3	111.7	-960.4	-4660.0	266/52
GPK3	112.2	-962.3	-4685.9	065/68
GPK3	112.3	-962.7	-4691.7	247/67
GPK3	112.3	-968.2	-4992.8	249/40
GPK3	111.8	-966.7	-4943.0	292/58
GPK3	111.2	-966.7	-4971.3	356/48
GPK4	280.6	-1590.0	-4635.0	275/73
GPK4	282.1	-1596.5	-4666.4	285/73
GPK4	282.8	-1600.3	-4683.6	275/77
GPK4	284.7	-1610.3	-4732.6	315/70
GPK4	287.1	-1623.3	-4826.3	255/74
GPK4	287.3	-1626.2	-4847.0	270/76
GPK4	287.6	-1632.0	-4886.9	250/67
GPK4	287.7	-1637.1	-4920.8	070/68
GPK4	287.7	-1638.3	-4929.0	350/75
GPK4	287.7	-1640.8	-4944.4	285/75
GPK4	287.6	-1641.3	-4947.2	280/74

Please note, that a slightly revised selection especially of the GPK3 fracture dataset has to be accounted for in future calculations.
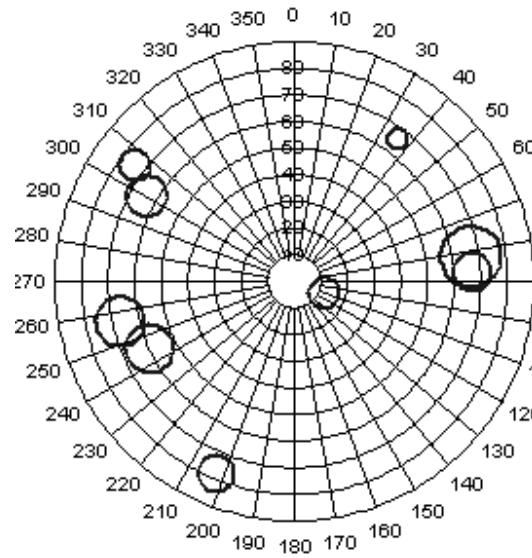
Fig. 6: *Dip and azimuth of dip of the stochastically positioned fracture zones. The size of the circles represent the relative occurrence in the model.*

3 PREPARATORY INVESTIGATION USING GPK3 STIMULATION DATA

It was envisaged to test the predictive applicability of the HEX-S code using the hydraulic stimulation of GPK4 in September 2004. Neither stimulation nor long-term monitored hydraulic data from the realm of GPK4 have been available. Therefore the capabilities of our approach could only be tested with data from the other boreholes. Since GPK2 fracture data are only rough estimates obtained from flow logs or from characterizations at different depth ranges, but not from image data in the open hole section, the only reliable information stems from GPK3. Here, half a year after finishing drilling activities, the borehole had been stimulated along the open hole section between 4487 and 5031 m TVD.

The major hydraulic stimulation test, 03MAY27, started on 27 May 2003 at 12:50 at GPK3. The total injection period lasted until June 7th, however, the treated time span for the preparatory investigations of the HEX-S model covers the first 530'000 s (>6 days). Flow rate was varied in numerous steps, starting with 30 l/s at the first day. In a first phase, flow was stepwise reduced to 20 l/s until 170'000 s, then reestablished at 30 l/s until 280'000s and finally set to 50 l/s, with a short-time (~3 hr) high injection rate of 70 l/s. The downhole pressure records had to be corrected using the borehole simulator HEX-B [23]. Pressure response was less pronounced with a first pressure level at $\Delta P = 10$ MPa that nearly continuously increased until $\Delta P = 16$ MPa at t = 530'000 s, irrespective of decreasing flow rate at early stage. The complete flow rate and (corrected) pressure record is shown in Fig. 7.

It needs to be stated clearly, that the goal of the preparatory investigations using GPK3 stimulation data was not a detailed reproduction of the downhole reservoir conditions. Due to the short time between code finalization and upcoming GPK4 stimulation test, the focus of the GPK3 test analysis was on the overall

reservoir behaviour. Therefore, no further data match has been conducted that would allow much more sophisticated characterisations. It is intended, to perform these characterizations in follow-up studies.

The hydraulic simulation results do not fully reflect the described smooth ΔP-behavior. However, the base level and short-term pressure variation are generally well reproduced (Fig. 7). Especially, positive flow steps are well represented (note pressure variation at t≈60'000s. 170'000s; and 290'000s). However, the pressure response at decreasing flow periods at the first stage is overestimated. A possible explanation is that due to the selected fracture parameters in the model the contribution of the irreversible shearing offset to aperture change is too high. This anticipates stronger transmissivity reductions at decreasing flow than measured. Another impact might arise from the choice of the boundary condition. Very probably, the boundaries are less permeable than assumed – this effect could be strongly responsible for the continuous increase in pressure. However, the strong non-linear hydraulic behavior is especially well described. The measured values propose a clearly non-linear flow regime; the increase of flow rate by 70% (29 to 50 l/s) results in a 30% pressure increase only. The HEX-S simulation reproduces this effect quite adequately. Another most important effect is the over-all little increase of borehole injectivity. Normalizing the pressure/flow record at an arbitrary 100% level at the end of the first flow step at injection, our model describes a final relative injectivity of 125% at t≈530'000s. Although the measured data indicate only 101% for the same time period, the agreement is remarkable: considering the strong "cubic law" relation between aperture change and permeability, completely different orders of magnitude could easily result.

Noteworthy is the effect of anisotropic flow elucidated by further sensitivity investigations. The flow pattern spreads first radially around the borehole, but is rapidly directed along the orientation of the major permeable structures. This could cause strong lateral pressure variations in the matrix, an effect that is also well known from the analysis of seismic locations.

The HEX-S parameters derived from the GPK3 data and used for the prediction of the GPK4 stimulation are given in Table 2x.

Table 2: Parameters of the HEX-S model derived from the GPK3 data and used for the prediction of the GPK4 stimulation

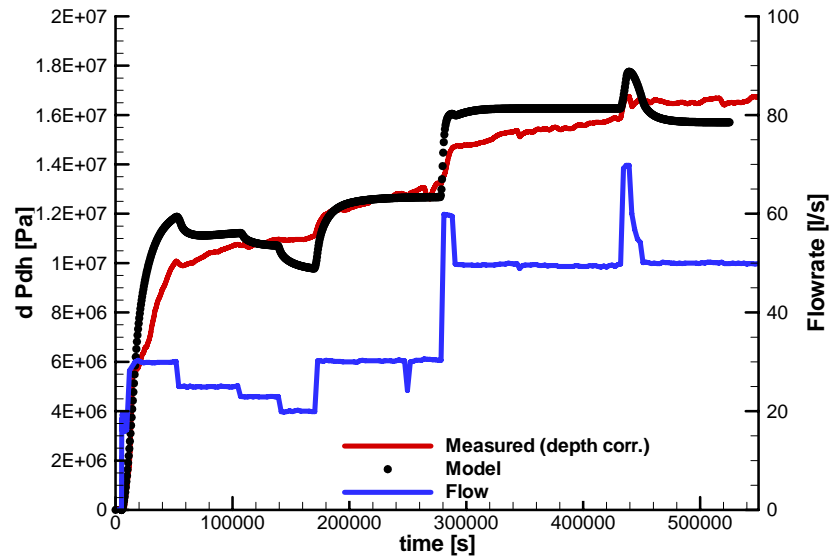| Fracture zones	slip patch radii	R	m	40
	fracture zone radii		m	80 – 180
	fracture shear stiffness	K_s	Pa m^{-1}	1.37 10^9
	90%-closure stress	$\sigma_{n,ref}$	Pa	3 10^7
	friction angle	Φ	°	34 (BH intersecting determ. fracs.)
				34 (stochastic. fracs.)
				37 (BH non-intersecting determ. fracs.)
	shear dilation angle	Φ_{dil}	°	3
	fracture zone density		m^{-1}	0.002
General	initial permeability	κ	m^2	5 10^{-17}

Fig. 7: *Hydraulic data from stimulation of GPK3 starting 27. May 2003, 12:50. Pressure data are provided as differential pressure (compared to ambient situation) by a red line, scaled by the left axis; flow rate (blue line) is given at the right axis. Also provided are the modelled differential pressure data (frequent black dots).*

Seismicity was strongly evolving starting next to the open hole section. Already after the first day, the seismic cloud was spread to a distance of >500 m (see also [16] for details). The general pattern of seismicity is directed in ~N-S direction, in agreement with the direction of the maximum horizontal stress component. The induced shearing events simulated by HEX-S (under pure normal stress regime) also tend to spread in N-S direction. In HEX-S, fractures with optimum orientation to the stress field for failure can shear in several subsequent time steps. This may cause slip displacements too small for having any seismic implication. At Soultz no measurements are recorded that fall below a seismic threshold of M< -1. Considering only shear displacements of more than 0.5 cm, the simulated shear failures are in good agreement with the located seismic events, however slightly different slippage threshold do not produce a strongly different pattern.

Our calculations for the GPK3 test 03MAY27 have revealed the high sensitivity of the model assumptions to the stress field. Initially, a transfer from a normal stress regime (σ_V being the main stress component) to a strike-slip regime (σ_H being the main stress component) at ~3000m has been assumed interpolated from single stress measurements using packer technology. Although initially stable at zero pore pressure, many of the deterministic and stochastic fracture zones at all boreholes would fail already at minor hydraulic pressure variations. It was a conclusion from the HEX-S modeling of test 03MAY27 that even a vague fit of the seismic observations couldn't be obtained. However, a much more reliable and robust situation evolved when assuming a normal stress field throughout the model depth down to 6 km. Therefore all our calculations and conclusions have been based on a normal stress field as follows:

SH_{max} [MPa] = 99.1 + 0.021*(z - 4750)

Sh_{min} [MPa] = 71.3 + 0.0159*(z - 4750)

Sv [MPa] = 117.7 + 0.0255*(z - 4750)

Azimuth of SH_{max} = 170°

As consequence of these rough modelling efforts it can be stated that HEX-S is well able to reproduce spatial constants of shear events that are similar to the extension of a microseismic cloud. This, again, is a clear indication that the simulated pressure field development in the rock matrix is adequately represented in HEX-S.

4 PREDICTION OF RESERVOIR BEHAVIOUR FOR GPK4 UNDER STIMULATION CONDITIONS

4.1 Background

The model runs performed on the GPK3 data of the stimulation test 03MAY27 represented the basis for the prognosis of the planned GPK4 stimulation. Due to a limited preparation time, the calculations should concentrate on the short-term stimulation effects rather than on the long-term system behavior. This goal is in agreement with the experience gained from 03MAY27 when both, the early spatial development of the seismic cloud (t<1-2 days) and the downhole overpressure have been adequately explained. The predictive approach for the planned stimulation of GPK4 should account for the hydraulic conditions revealed by the preliminary 0.7 l/s low rate injection test 04SEP08. It was intended that the HEX-S prediction provides a conclusive physical model that includes the characteristics of the seismic and hydraulic stimulation results.

From the initial injection test 04SEP08 it was concluded that the matrix permeability at GPK4 is generally rather small, compared to earlier evaluations at Soultz [24]. The value used in our approach (k=10^{-16}m^2) is however not very sensitive to the overall hydraulic behavior. The key factor is the number and property of fractures intersecting each borehole. Different model calibration runs have been realized to scale the apertures of the fractures to reproduce the initial hydraulic borehole transmissivity derived from the test 04SEP08. Also for GPK4, the fracture data from Table 1 were used.

A first stimulation prediction has been submitted to the Soultz project partners on the morning of 13 Sep 2004, a couple of hours after the start of the stimulation GPK4 test 04SEP13 [25]. This included especially the results discussed below in Chapter 4.2.

4.2 Hydro-mechanical prediction of stimulation GPK4

This Chapter includes a slightly more elaborated description of the forecast, however, keeping the modeling results submitted immediately after the start of test 04SEP13 unchanged. The prediction was based on model runs with slightly varying parameter sets. Out of these runs, Model "C" has been considered to be most reliable. The difference between the runs has been the RVFI in the case of runs "C2" and "C3", and the stress field applied in the case of "B". Especially, Model "C" produced the most robust shearing events using a normal stress field (see remarks in Chapter 3), whereas Model "B"

assumed a stress transfer from normal to strike slip resulting in strong shearing activity at already minor pore pressure changes.
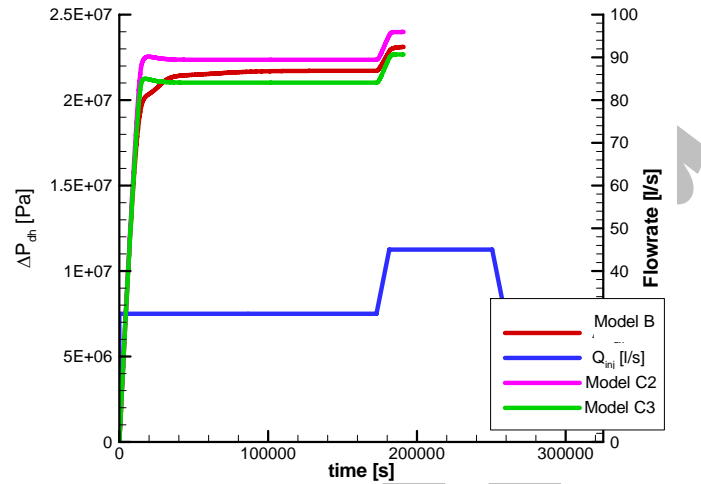

Fig. 8: Predicted hydraulic pressure development at GPK4 for a stepwise 30/45 l/s injection at GPK4. For the models C2/C3 a maximum peak at the beginning occurs at t=15500 s; Model B (based on a slightly different geometry) did not produce any characteristic peak in the start phase. Calculations assume an instantaneous start of the 30 l/s flow rate.

Instantaneously at the beginning of the injection all models predicted an immediate increase of the downhole pressure. The pressure stabilized at a pressure difference (compared to hydrostatic conditions) at a level between $\Delta P = 20$ MPa to 24 MPa for the planned injection rate of 30l/s (Fig. 8). When increasing flow to the second planned rate of 45 l/s an additional pressure increase of 1.5 MPa would result. The models "C2" and "C3" predict a maximum pressure peak at the beginning at t=15500 s whereas Model "B" did not produce any characteristic peak in the start phase. Compared to the low rate injection test the injectivity would have been increased by more that a factor >5. In conclusion it was stated that even higher flow rates still would significantly improve the hydraulic conditions at GPK4.

The shearing events were predicted to occur mostly at the bottom part of GPK4. As stated earlier, the strong inclination of GPK4, yields here a ~100m distance between real to modeled structures that have to be accounted for in the subsequent considerations. Correcting the locations of the modeled events (Fig. 9) requires a shift of maximum 100 m south (at the bottom part of GPK4, south is right in the perspective of Fig. 9). They will then be placed around the bottom part of the open-hole section of GPK4.

For the first 10 hrs of the stimulation test (Fig. 9) shearing is forecasted to occur within a radius of 100 m around GPK4 at $z \approx -4900$m ($\Delta z=\pm75$m) and extending towards greater depths. During a next time interval (t<1day, see Fig. 10), the forecasted cloud will move slightly upwards (+100m). Generally fracture failure tends to move towards the already stimulated areas next to GPK3, as well as along the large fault zones located by Maurer [22] from earlier microseismic activity, which are not intersected by any borehole. The events next to GPK4 continue to migrate upward.
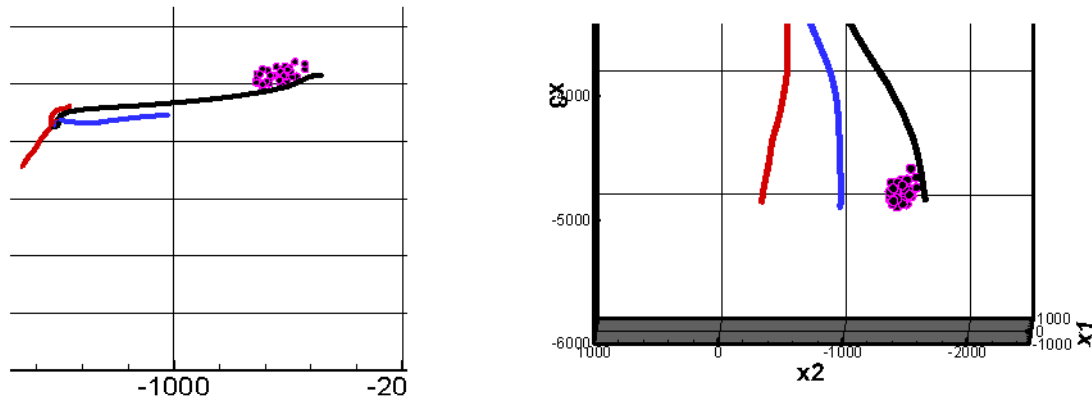
Fig. 9: Predicted microseismic evolution at GPK4 within the first 10h interval after stimulation start (left: plane view, right: view from west). The lines represent the real borehole trajectories (black GPK4, blue GPK3, red GPK2).
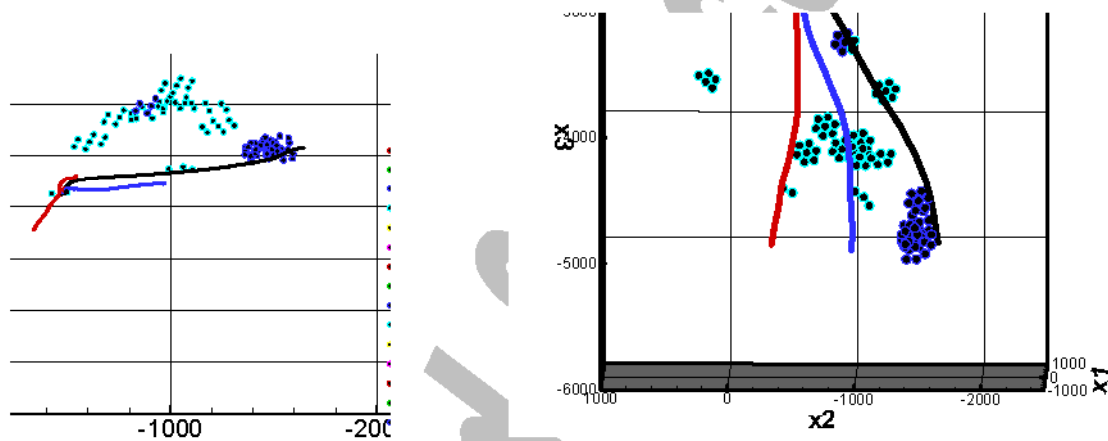

Fig. 10: Predicted microseismic evolution at GPK4 within the 1ˢᵗ day after stimulation start (left: plane view, right: view from west). Shearing threshold was set to 1 cm.

Under the ambient stress field the stochastic fractures are partly critically stressed. Due to the still ignored effects of fracture cohesion, shear failure will occur at the smallest perturbation in the matrix. This is shown in Fig. 10 by the off-borehole shearing clusters towards the East. However, most deterministic fractures are only near-critically stressed and will start shearing only if a substantial pressure perturbation occurs.

4.3   Measured data from stimulation 04SEP13

The stimulation experiment 04SEP13 has been conducted over 4 days from 13 to 16 Sep. 2004, using mostly a injection rate of 30 l/s. Fig 11 shows the difference of the measured pressure to hydrostatic pressure and the flow rate history. The pre-stimulation downhole pressure at 4700 m depth (MD) was

~46.2 MPa, that includes still the declining trend from the shut-in at the end of the earlier 04SEP08 test. Just before the start of 04SEP13 the hydrostatic pressure was approached slowly at a rate of < 0.03 MPa/hr (or < 0.7 MPa/day). To compare the measurements with the predicted results, the overpressure is assumed to have a constant pressure effect of 2.8 MPa above the initial hydrostatic pressure (43.4 MPa). Maximum absolute downhole pressure in the first 30 l/s injection flow period reached 61.5 MPa in 4700 m depth within 10000 s after injection start. After that, a pressure decline of 0.023 MPa/hr occurred that certainly includes the effect of the superimposed declining trend from the test 04SEP08. 49 hr after injection started, the flow-rate was increased three times to the planned second step of 45 l/s, however the pumping system could not provide these flow rates over more than 1.5 hr periods. The downhole data indicate an additional pressure increase of about 1 MPa at the end of each period.
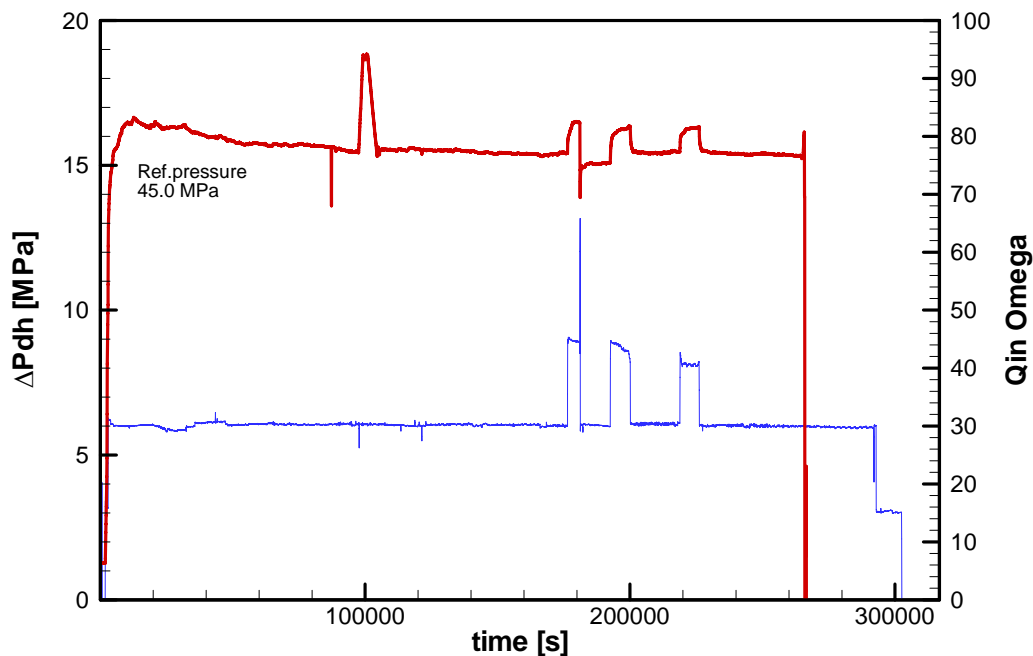

Fig 11: Downhole pressure and flow rate during 04SEP13 between 13-16 Sep. 2004. Reference time (t=0) is 13 Sep 2004 08:00.

During the whole test more than 15'000 events have been recorded using the downhole measurement net at Soultz (Baria et al. [26]). At present >5700 events have been located. Fig. 12 (left) illustrates that the seismic activity started at the bottom of the borehole GPK4 in the first 10 hrs of injection. From Fig. 12 (right) the seismic density of all measurements until 25 Sep can be recognized that include also events triggered during the shut-in phase. Seismicity has gradually developed northwards towards GPK3 and upwards towards the casing shoe in 4489 m TVD.
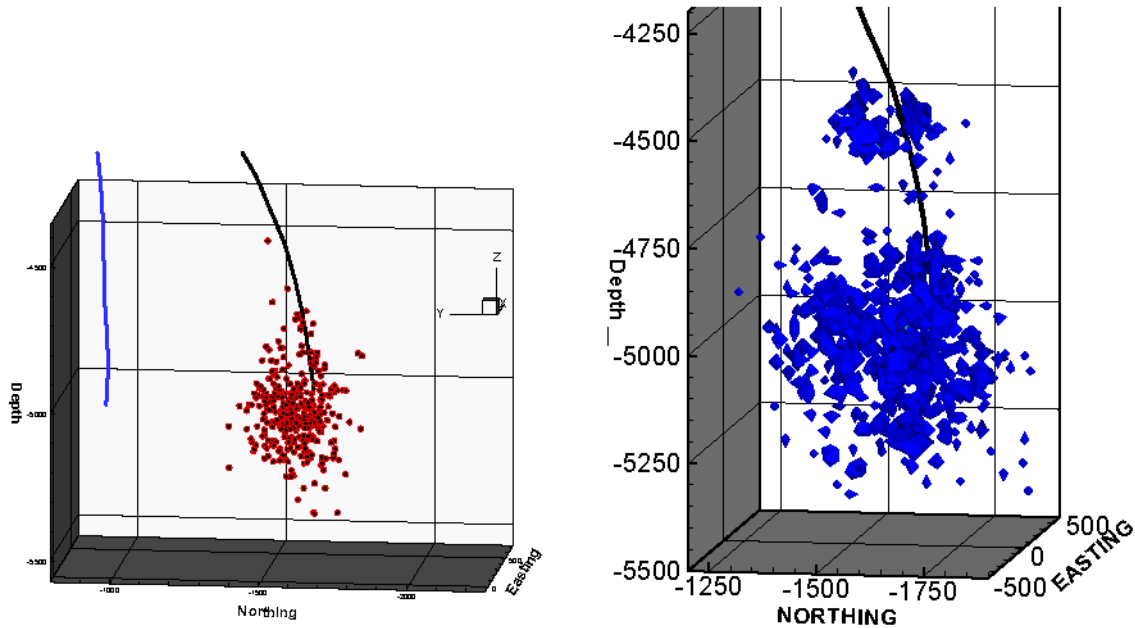
Fig. 12: Seismicity at GPK4 during the first 10 hr stimulation (left) and seismic density (right) over the total stimulation period until 24 Sep 2004 (GPK4 black, GPK3 blue line). Seismic density isosurface represents values above $8x10^{-5}$ events/m^3.

4.4 Discussion

A challenging task of a prediction of the complex hydromechanical interactions in the reservoir for the GPK4 stimulation test 04SEP13 has been conducted. The overall hydraulic and microseismic behavior was predicted immediately the stimulation test started. The subsequent comparison with measured data did not indicate principal inconsistencies. For the first 10 hr stimulation period the forecast resulted in an extraordinarily precise simulation of the seismic pattern, including both, spatial location and spatial evolution. Nevertheless, the predictions will be investigated in more detail under the light of the measurement data from 04SEP13.

The hydraulic overpressure was overestimated by ~30%. However, the dynamic system responses show particular agreements: 1) the major shearing events at the beginning of the test at 10'000 s were nearly perfectly forecasted and 2) the additional pressure increase when increasing flow rate by 50% (30 to 45 l/s) was predicted nearly as measured. The model used lateral Dirichlet boundary conditions that apparently provide a good estimation of the real field conditions. It may be noted that the GPK3 test would be probably better characterized by more complex boundary conditions.

Fig. 10 illustrates that also in the first phase of injection the simulated fracture failures do not necessarily occur in the borehole vicinity. These events are linked to strongly critically oriented slip patches. The implementation of an initial shear resistance or the assignment of higher shear friction angles could reduce immediate shear failures.

At later stages of the test (t>1day) there are more differences occurring between measured and forecasted events. This is certainly due to assumptions on major far-field connecting fault zones. Under

the conditions of Soultz these fault zones certainly play a major role but they are difficult to locate. In order to improve the quality of such predictions, a careful analysis of existing microseismic events is required. It is intended to advance in this direction by performing an iterative procedure that includes a seismic density analysis.

The initial apertures of the "stochastic" slip patches in the model C3 range from 2.0×10^{-5} to 3.0×10^{-4} m, depending on the orientation and depth (Fig. 13). Most slip patches of the deterministic fracture zones have generally larger apertures that are derived from scaling the borehole transmissivity. The latter process applies on well-conductive (Fig. 13) deterministic structures identified in the microseismic clouds from the GPK2 and GPK3 stimulation tests.
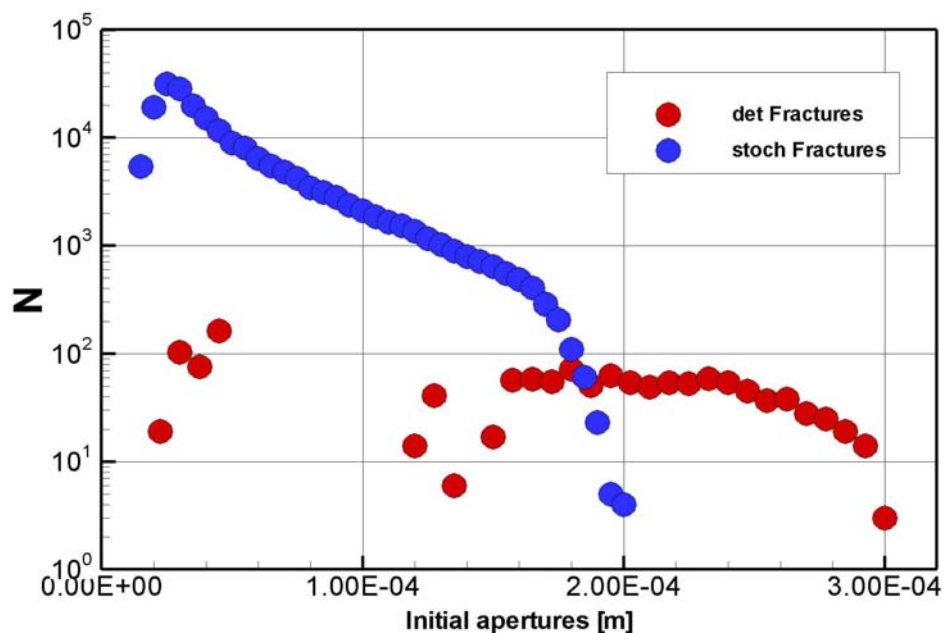

Fig. 13: Frequency of the initial apertures of the deterministic and stochastic slip patches in the model C3

During the first phase of the stimulation (30 l/s) the model C shows an additional fracture volume of around 1000 m^3 reached 1 day after the stimulation start (Fig. 14). Increasing the flow rate to 45 l/s at t=180'000 s leads to an increase of the new fracture volume to over 1500 m^3. This linear behaviour between flow rate and new fracture volume is not reflected in the wellhead pressure where only an increase of 10% was calculated. This is due to the fact that the aperture increase is limited generally to a radius of 1800 m. The increase remains constant already after some few hours of injection and is associated locally by an increase of the dynamic pressure field focussing to higher transmissive paths. A maximum enhancement of the apertures by a factor 5-6 was calculated in the vicinity of the borehole GPK4 and a factor of < 4 further to the boundary of the reservoir. The shear displacement failure of the slip patches can create locally next to the borehole up to 70% of the total aperture enhancement. This becomes obvious in Fig. 15 when comparing the general level of displacements of approx. 0.01 m in the reservoir domain to the maximum values of 0.015 m in the vicinity of the borehole. It is however

worthwhile to be noted that over 80% of the new fracture volume during stimulation is generated by the compliance process, which will disappear after the injection has stopped and the overpressure has vanished. (Fig. 14, left).
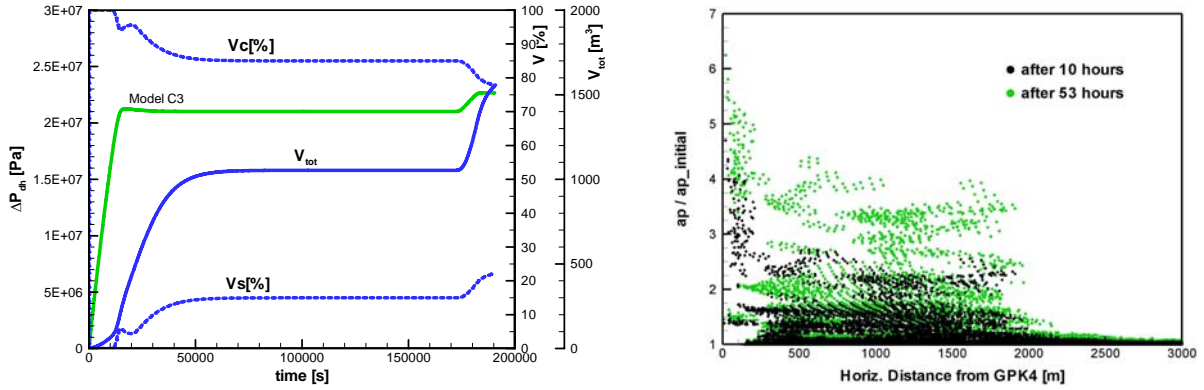

Fig. 14: Left: Calculated development of new fracture volume during the stimulation of GPK4 with model C, given in total m³ and the percentage of the compliant and shearing part. Right: Factor of total aperture change as a function of the horizontal distance to GPK4 after 10 and 53 hrs when flow rate has been increased by 50%.
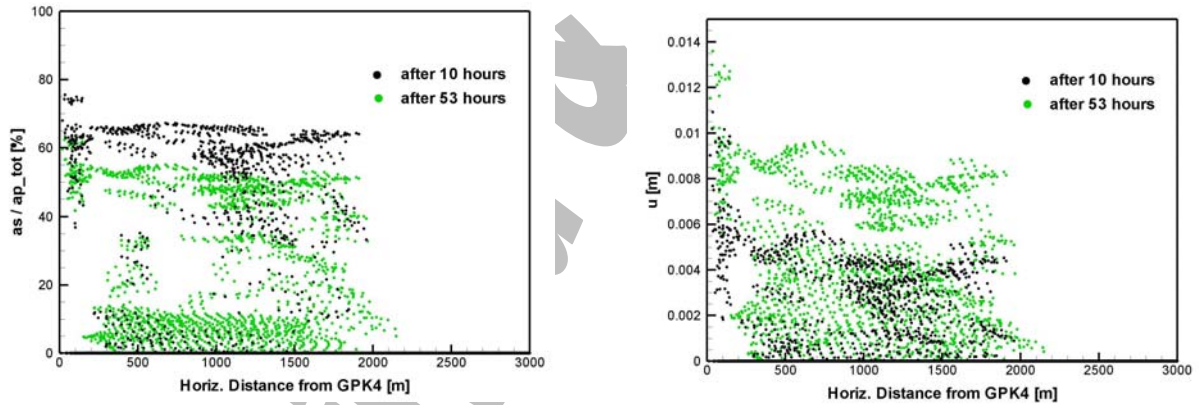

Fig. 15: Left: Percentage of predicted aperture enhancement by shearing with model C. Right: Predicted shear displacements with model C.

It is not envisaged to accomplish an analysis of the hydraulic structures in Soultz in this paper. It just can be stated that the microseismic events are finally the result of the in-situ fracture pattern but also from hydraulic flow conditions (transmissivity and boundary conditions). In a synthetic analysis, Fig. 16 illustrates the possible effect of transmissivity development through mechanical stimulation. The spatial isosurfaces illustrate the increase of a 0.1 mm fracture aperture that starts from the injection borehole. The shape of these surfaces may extent to large distances and becomes very complex with time, but the highest impact is clearly in the vicinity of the boreholes within the inner reservoir.
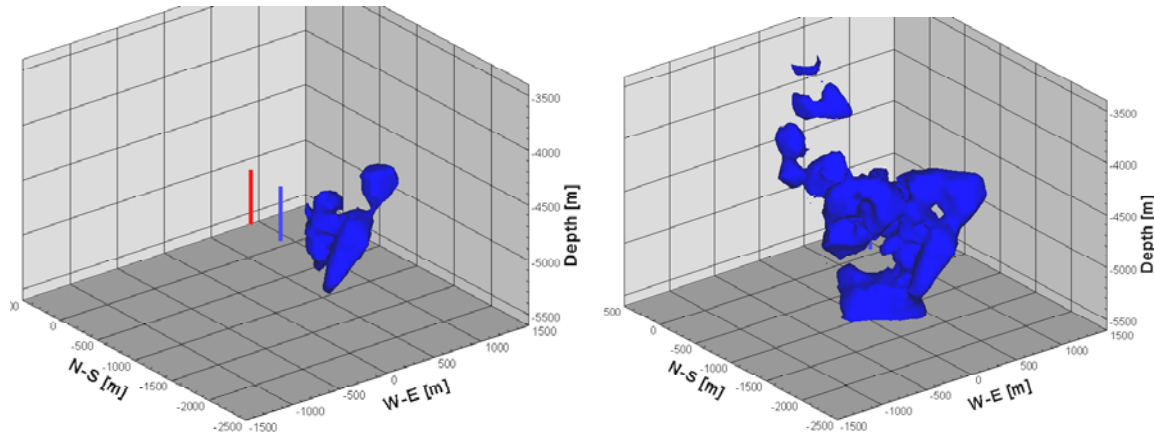
Fig. 16:   Calculated iso-surface of the 0.1 mm fracture aperture after 5 hours (top) and 20 hours (bottom) of injection into GPK4 for the 5 km deep reservoir domain at Soultz-sous-Forêts

5   CONCLUSION

The new hydro-mechanical reservoir model HEX-S has been tested on data from the stimulation of the 5 km deep reservoir of European EGS project site in Soultz-sous-Forêts (France). A post-stimulation interpretation of the GPK3 data as well as a predictive modeling of the hydro-mechanical reservoir behavior for the GPK4 stimulation have been successfully carried out.

The model allows an insight into the complex and transient behavior of a fractured reservoir under massive flow injections during stimulation. HEX-S generates a physical reservoir model considering the time-dependent evolution of the hydraulic field and changing fracture apertures. The processes of permeability development are implemented as a combination of reversible and irreversible aperture variations of deterministically and stochastically defined fractures. Irreversible aperture changes are based on shearing failures. This allows not only interpreting pressure response data but also locations of microseismic events. A further important aspect is that the simulation of the dynamic reservoir behavior is strongly based on a combined data analysis integrating lithological, hydraulic, thermal and stress information.

The current experience thus demonstrates that the new HEX-S tool is especially well suited to

- Forecast the early (t < 1 day) hydraulic and seismic behaviour
- Explain the major processes responsible for the induced microseismicity

This limitation of the model response due to geological uncertainties can only be prevailed by performing more stochastic calculations and re-adapting the model during a running stimulation test. On the other hand, the accuracy of the implemented processes in the HEX-S model can be presented by the fact of the linear dependency of fluid injection volume to the total volume increase in the matrix. In the constitutive laws this relation is not explicitly formulated, should however be intrinsic. The model results

discussed in Chapter 4.4 reproduces nearly exactly this behaviour. Targeting the areas of major volume increase by additional boreholes could certainly help to improve the efficiency of stimulation tasks. Therewith, our model can lay the basis for the understanding of the physical complexity that occurs during hydraulic stimulation of a fractured rock matrix.

The calculation of this coupled hydro-mechanical interaction provides perspectives for future applications such as design calculations for optimizing cost-intensive hydraulic stimulation strategies before hand under financial or logistical restrictions. Therewith it is also possible to test and quantify new reservoir creation strategies like dual-injections as proposed by Baria et al. [26] at a given site. Since the EGS technology is usually coupled at populated areas predictive quantification of hydro-mechanical processes in the reservoir domain under stimulation is of specific interest.

6 ACKNOWLEDGEMENTS

7 REFERENCES

1.   LeCarlier, C., J.-J. Royer, and E.L. Flores, *Convective heat transfer at the Soultz-sous-Forets geothermal site; implications for oil potential.* First Break, 1994. **12**(11): p. 553-560.

2.   Pribnow, D., et al. *The European HDR project in Soultz: An unconventional reservoir type?* 1999. Geothermal Res. Council Transactions.

3.   Kohl, T., D. Bächler, and L. Rybach. *Steps towards a comprehensive thermo-hydraulic analysis of the HDR test site Soultz-sous-Forêts.* in *World Geothermal Congress 2000.* 2000. Kyushu-Tohoku, Japan.

4.   Baria, R., et al. *The European HDR programme: main targets and results of the deepening of the well GPK2 to 5000 m.* in *Proc. World Geothermal Congress 2000.* 2000. Japan.

5.   Gérard, A., *Stimulation hydraulique du puit GPK3 et tests de circulation entre les puits GPK3 et GPK2 - Note de synthèse.* 2004, Rapport ADEME / GEIE "Exploitation Minière de la Chaleur No. 01.05.030.

6.   Kohl, T. and T. Mégel. *Coupled Hydro-mechanical modelling of the GPK3 reservoir stimulation at the European EGS site Soultz-sous-Forêts.* 2005. 30th Workshop on Geothermal Reservoir Engineering, Stanford University, Stanford, California, January 31-February 2, 2005.

7.   Barton, C.A., M.D. Zoback, and D. Moos, *Fluid flow along potentially active faults in crystalline rock.* Geology, 1995. **23**(8): p. 683-687.

8. Segall, P., *Earthquakes triggered by fluid extraction.* Geology, 1989. **17**: p. 942-946.

9. Maillot, B., S. Nielsen, and I. Main, *Numerical simulation of seismicity due to fluid injection in a brittle poroelastic medium.* Geophys. J. Int., 1999. **139**: p. 263-272.

10. Cuenot, N., C. Dorbath, and L. Dorbath, *Analysis of the microseismicity induced by fluid injections at the Hot Dry Rock site of Soultz-sous-Forêts (Alsace, France): implications for the characterization of the geothermal reservoir properties.* Pure and Applied Geophysics, 2006. **in press**.

11. Bruel, D. *Modelling hydraulic jacking tests on a pre-existing fracture system.* in *Proc. Int. Congress on Rock Mechanics (Int. Soc. for Rock Mech.).* 1999.

12. Baujard, C. and D. Bruel. *Improving a numerical tool and evaluating impact of density changes of injected fluids in the hydraulic behavior of HDR reservoirs.* in *30th Stanford Geothermal Congress, Stanford, California, US.* 2005.

13. Shapiro, A., J.J. Royer, and P. Audigane, *Large scale in-situ permeability tensor of rocks from induced microseismicity.* Geophys. J. Int., 1999. **137**: p. 207-213.

14. Kohl, T., et al., *Coupled hydraulic thermal and mechanical considerations for the simulation of Hot Dry Rock reservoirs.* Geothermics, 1995. **24**(3): p. 333-343.

15. Cornet, F.H. and Y. Jianmin, *Analysis of Induced Seismicity for Stress Field Determination and Pore Pressure Mapping.* Pageoph, 1995. **145**(3/4): p. 677-700.

16. Asanuma, H., et al. *Data Acquisition and Analysis of Microseismicity from the Stimulation at Soultz in 2003 by Tohoku University and AIST, Japan.* in *Geothermal Resource Council, Palm Spring Sep. 2004.* 2004.

17. Evans, K.F., et al., *Microseismicity and permeability enhancement of hydrogeologic structures during massive fluid injections into granite at 3 km depth at the Soultz HDR site.* Geophys. J. Int., 2005. **160**: p. 388-412.

18. Willis-Richards, J., K. Watanabe, and H. Takahashi, *Progress toward a stochastic rock mechanics model of engineered geothermal systems.* Journal of Geophysical Research, 1996. **101**(B8): p. 17,481-17,496.

19. Jing, Z., et al., *A 3-D water/rock chemical interaction model for prediction of HDR/HWR geothermal reservoir performance.* Geothermics, 2002. **31**: p. 1-28.

20. Bächler, D., et al., *Data Analysis and controls towards understanding reservoir behaviour and the creation of a conceptual model.* 2001, Final Report to the Bundesamt für Bildung und Wissenschaft, Projekt 98.0008-1 - EU Project No. JOR3-CT98-0313: Bern, Switzerland.

21. Kohl, T. and R.J. Hopkirk, *"FRACTure" a simulation code for forced fluid flow and transport in fractured porous rock.* Geothermics, 1995. **24**(3): p. 345-359.

22. Maurer, R., *Erstellung von Kluftmodellen und vergleichende hydraulische Modelle des geothermischen Reservoirs von Soultz-sous-Forêts.* 2004, Diploma Thesis Univ. Freiburg (D). p. 95.

23. Mégel, T., et al. *Downhole pressures derived from wellhead measurements during hydraulic experiments.* in *Proceedings World Geothermal Congress 2005.* 2005. Antalya, Turkey.

24. Jung, R., et al. *Evaluation of hydraulic tests at Soultz s.F., European HDR site.* 1995. Proc. World Geothermal Congress, Florence, Italy.

25. Kohl, T. and T. Mégel, *Short Note on 1st Stimulation Phase of GPK4 during 13-16 September 2004: Prognosis and Conclusion.* 2004, Int. report to E.E.I.G. Soultz-sous-Forêts. p. 9.

26.   Baria, R., et al. *Microseismic monitoring of the world s largest potential HDR reservoir.* in *29th Workshop on Geothermal Reservoir Engineering Stanford University, Stanford, California, January 26-28, 2004.* 2004.